Supplement of Geosci. Model Dev., 15, 6143–6164, 2022
https://doi.org/10.5194/gmd-15-6143-2022-supplement

Geoscientific
Model Development

Supplement of

Simulations of aerosol pH in China using WRF-Chem (v4.0): sensitivities of aerosol pH and its temporal variations during haze episodes

Xueyin Ruan et al.

Correspondence to: Lei Geng (genglei@ustc.edu.cn) and Chun Zhao (chunzhao@ustc.edu.cn)

Text S1. Comparison of $PM_{2.5}$ pH predictions between MOSAIC and ISORROPIA II

To further explore the potential effects of different thermodynamic models on the modeled aerosol pH differences between this study and previous studies, we also compare the MOSAIC results with those obtained from ISORROPIA II. The WRF-Chem simulated hourly chemical concentrations along with temperature and RH in Beijing from CTL3meta scenario are used as inputs to ISORROPIA II (forward mode, assuming metastable to be consistent with CTL3meta). Time series of aerosol pH (bin 01–bin 06) predicted by the two different models are given in Fig. S9. Overall, ISORROPIA II and MOSAIC predict a similar temporal pH trend, but ISORROPIA II in general predicts higher absolute pH values than that of MOSAIC for all particles with the size less than 2.5 μm. What is more, a regression slope of 0.87 between the calculated $PM_{2.5}$ pH by MOSAIC and ISORROPIA II is found (Fig. S10). These findings are comparable to the results reported by Pye et al. (2020) who found that with the same model inputs, a regression slope of 0.89 between the calculated pH from the box-model version of MOSAIC and ISORROPIA II was obtained. Comparisons of the pH values predicted by MOSAIC and ISORROPIA in Zaveri et al. (2008) also showed a similar phenomenon that ISORROPIA tended to predict higher values under same conditions. The discrepancy between these two models may be attributed to the higher amounts of aerosol water content predicted by ISORROPIA II relative to MOSAIC, as indicated in Fig. S11, despite both models using the same phase state assumption and RH. Difference in other fundamental thermodynamic treatments, including activity coefficients, and solution approach may also account for the final pH difference. Nevertheless, the exact causes of the differences in pH predicted by these two models remain to be explored.

Table S1. Reaction rate expressions, rate constants (k) and ionic strength (I_s) effects for sulfate production in aerosol water.

Oxidants	Sulfate formation rate (M s^{-1})	Notes	References
O_3	$(k_1[H_2SO_3]+k_2[HSO_3^-]+k_3[SO_3^{2-}])[O_3(aq)]$		(Hoffmann and Calvert, 1985)
	$k_1 = 2.4\times10^4$ M^{-1} s^{-1}		
	$k_2 = 3.7\times10^5\times e^{(-5530\times(1/T-1/298))}$ M^{-1} s^{-1}		
	$k_3 = 1.5\times10^9\times e^{(-5280\times(1/T-1/298))}$ M^{-1} s^{-1}		
H_2O_2	$k_4[H^+][HSO_3^-][H_2O_2(aq)]/(1+K[H^+])$		(Mcardle and Hoffmann, 1983)
	$k_4 = 7.45\times10^7\times e^{(-4430\times(1/T-1/298))}$ M^{-1} s^{-1}		
	$K = 13$ M^{-1}		
	EF[a] =10(3.055log(I_s)-1.919)	$I_{s,\,max}$ = 14.5 M	(Liu et al., 2020)
NO_2	$k_5[S(IV)][NO_2(aq)]$		(Clifton et al., 1988; Lee and Schwartz, 1982)
	$k_{5low} = 2\times10^6$ M^{-1} s^{-1}		
	$k_{5high} = (1.24–2.95)\times10^7$ M^{-1} s^{-1}		
O_2	$k_6[H^+]^{-0.74}[S(IV)][Mn(II)][Fe(III)]$ (pH $\leq$ 4.2)		(Ibusuki and Takeuchi, 1987)
	$k_6 = 3.72\times10^7\times e^{(-8431.6\times(1/T-1/297))}$ M^{-2} s^{-1}		
	$k_7[H^+]^{0.67}[S(IV)][Mn(II)][Fe(III)]$ (pH > 4.2)		
	$k_7 = 2.51\times10^{13}\times e^{(-8431.6\times(1/T-1/297))}$ M^{-2} s^{-1}		
	$\log_{10}\left(\frac{k}{k^{I_s=0}}\right) = \frac{b_1\sqrt{I_s}}{1+\sqrt{I_s}}$	$I_{s,\,max}$ = 2.3 M b_1 = -3.02	(Liu et al., 2020)

[a] Enhancement factor accounts for the overall effects of ionic strength on the reaction rate constant k, Henry's law constants of H_2O_2 and SO_2, and the first-order dissociation constant of H_2SO_3. The expression was got by personal communication.

Table S2. The ranges and mean of surface $PM_{2.5}$ pH at sampling site in each scenario during clean, light pollution, moderate pollution, heavy pollution periods as well as the entire period.

Scenarios	Clean		Light		Moderate		Heavy		Entire period	
	range	mean	range	mean	range	mean	range	mean	range	mean
ORIG	1.1-7.1	3.2	1.1-6.8	2.1	1.0-2.6	1.6	0.9-2.5	1.4	0.9-7.1	2.3
CTL1	1.7-7.5	4.7	1.4-7.3	2.7	1.3-3.1	2.2	1.2-3.0	1.9	1.2-7.5	3.2
CTL2	2.4-7.5	5.0	2.2-7.4	3.6	2.3-3.8	3.3	2.1-3.8	3.1	2.1-7.5	3.9
CTL3	2.4-7.5	4.9	2.3-7.4	3.5	2.4-3.8	3.3	2.0-3.8	3.1	2.0-7.5	3.9
CTL3meta	2.4-7.7	4.8	2.3-7.3	3.4	2.4-3.6	3.2	2.1-3.6	3.0	2.1-7.7	3.8
CTL3het_NoIs	1.8-7.6	5.2	1.2-7.4	3.5	1.1-3.5	2.6	0.6-3.2	1.7	0.6-7.6	3.1
CTL3het_Is	2.3-7.7	4.9	2.2-7.4	3.5	2.4-3.7	3.2	1.9-3.7	3.0	1.9-7.7	3.8

Table S3. The concentrations (in unit of μmol m^{-3}) of major $PM_{2.5}$ components for each bin (01-06) averaged over the pH-decreasing regions (denoted by the blue box in Fig. 7) in CTL3meta scenario during the study period of 15 October 2014 to02 November 2014.

Size bin	Ca^{2+}	Na^{+}	SO_4^{2-}	NH_4^{+}	NO_3^{-}	Cl^{-}
bin 01	0.0001	0.0003	0.0006	0.0009	0.0001	0.0001
bin 02	0.0001	0.0003	0.0012	0.0020	0.0001	0
bin 03	0.0005	0.0006	0.0025	0.0036	0.0001	0.0001
bin 04	0.0032	0.0017	0.0025	0.0013	0.0006	0.0012
bin 05	0.0135	0.0053	0.0009	0	0.0035	0.0053
bin 06	0.0426	0.0164	0.0006	0	0.0061	0.0164

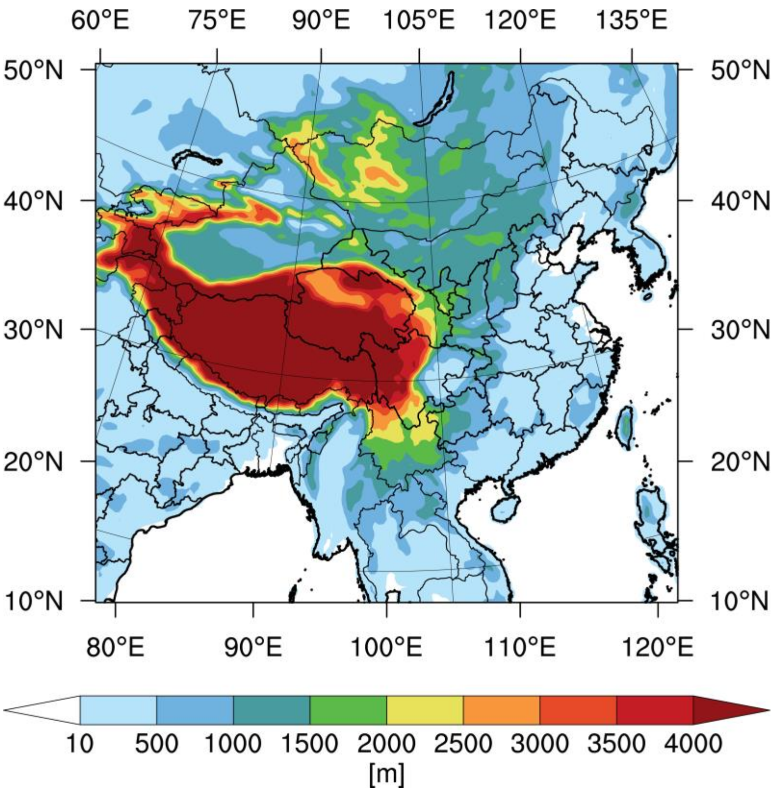

Figure S1. Simulation domain. The color shading represents the topography height (m).

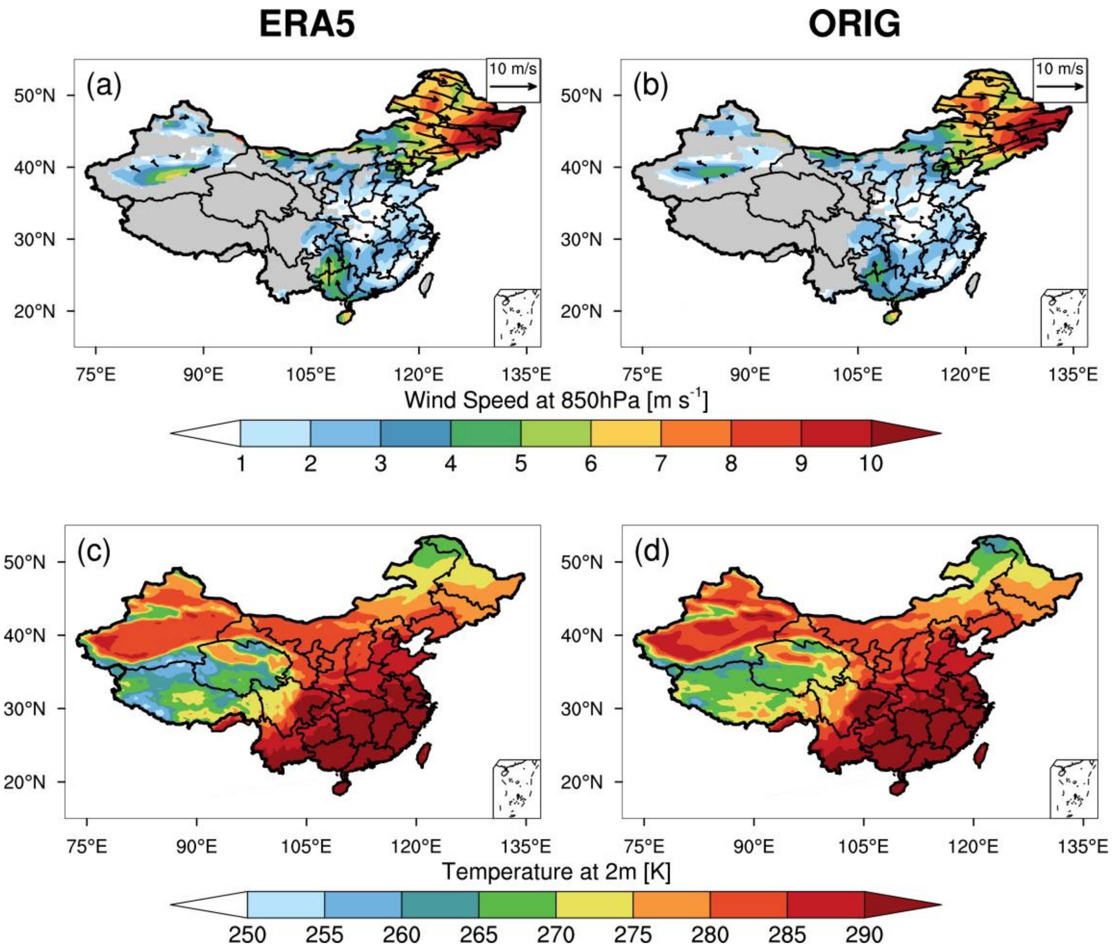

Figure S2. Spatial distributions of (a,b) wind speed at 850 hPa and (c,d) temperature at 2m from (left panels) ERA5 reanalysis datasets and (right panels) ORIG scenario averaged for the study period of 15 October 2014 - 02 November 2014.

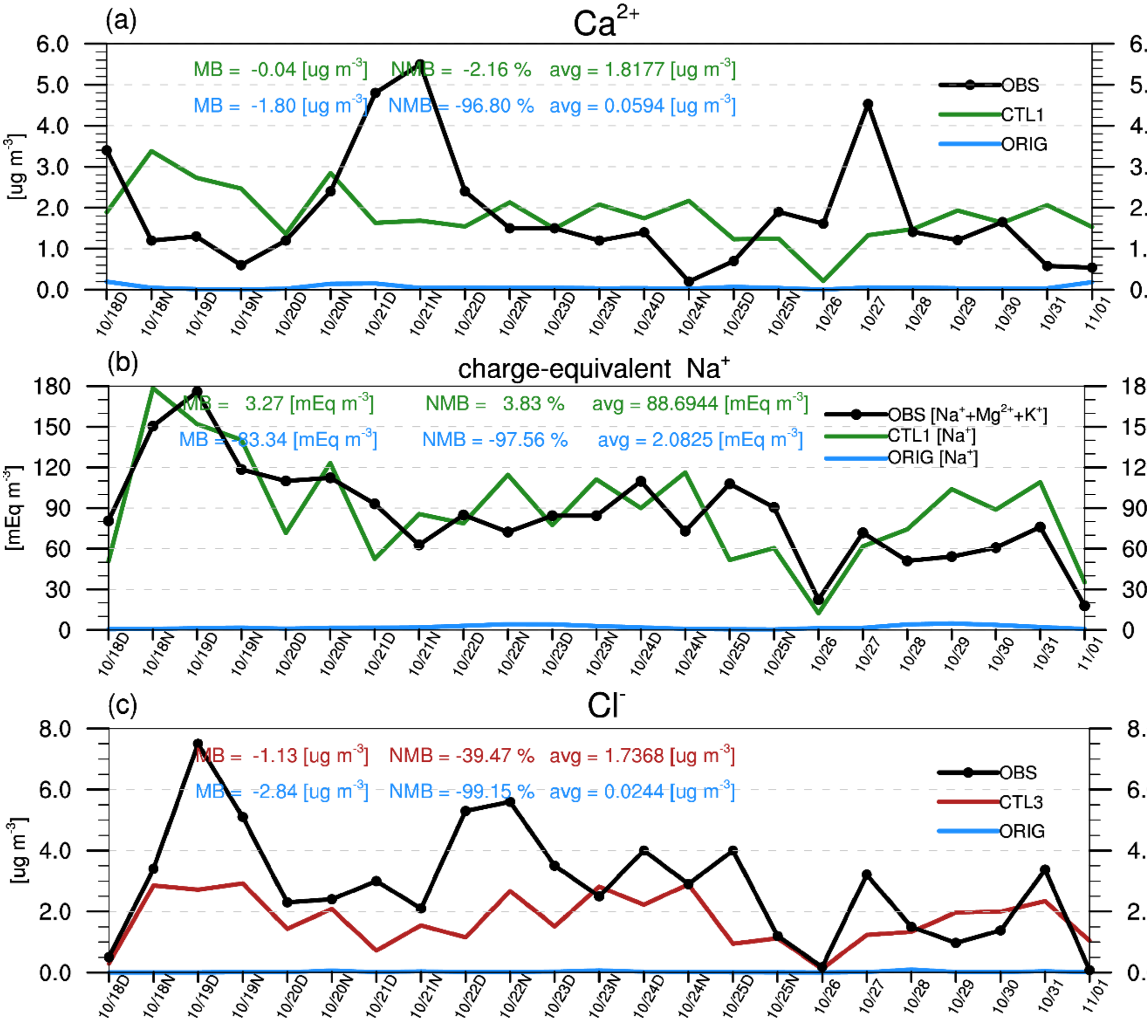

Figure S3. Comparison of simulated (a) Ca^{2+} concentration (μg m^{-3}), (b) Na^+ concentration (mEq m^{-3}), and (c) Cl^- concentration (μg m^{-3}) with observations (OBS; black line) for ORIG (blue line), CTL1 (green line), and CTL3 (red line) scenarios at Beijing site during the study period of 15 October 2014 - 02 November 2014, with the mean bias (MB), normalized mean bias (NMB) and average value (avg) given insert. MB and NMB are defined as $MB = \frac{1}{N}\sum_1^N C_m - C_o$ and $NMB = \frac{\sum_1^N C_m - C_o}{\sum_1^N C_o}$, where C_m is the modeled value, C_o is the observed value, and N is the number of paired model and observation data. Mg^{2+} and K^+ are treated as charge-equivalent Na^+.

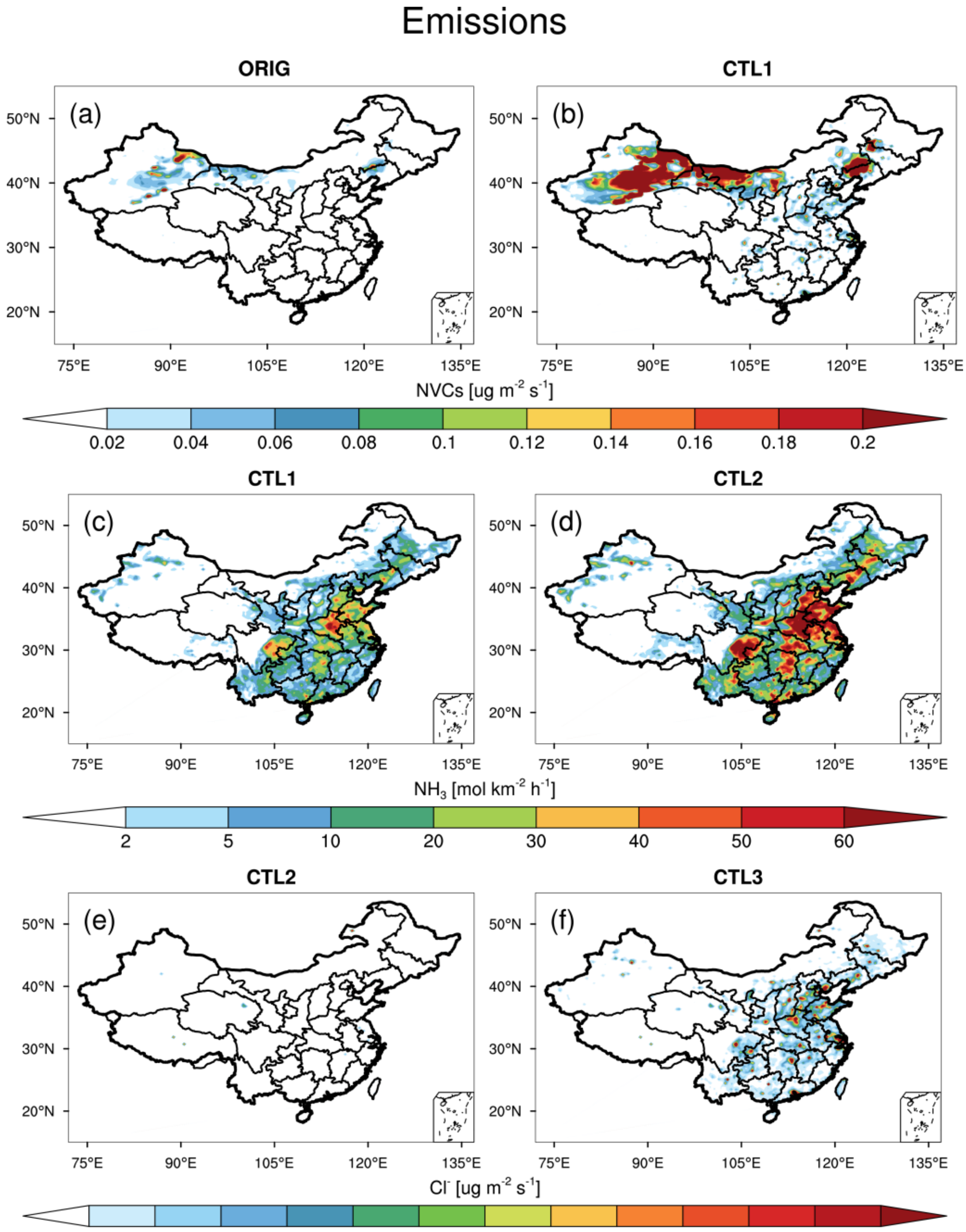

Figure S4. Spatial distributions of emissions of (top panel) NVCs, (middle panel) NH_3, (bottom panel) and Cl^- from default configuration and its corresponding sensitivity experiment during the study period of 15 October 2014 - 02 November 2014.

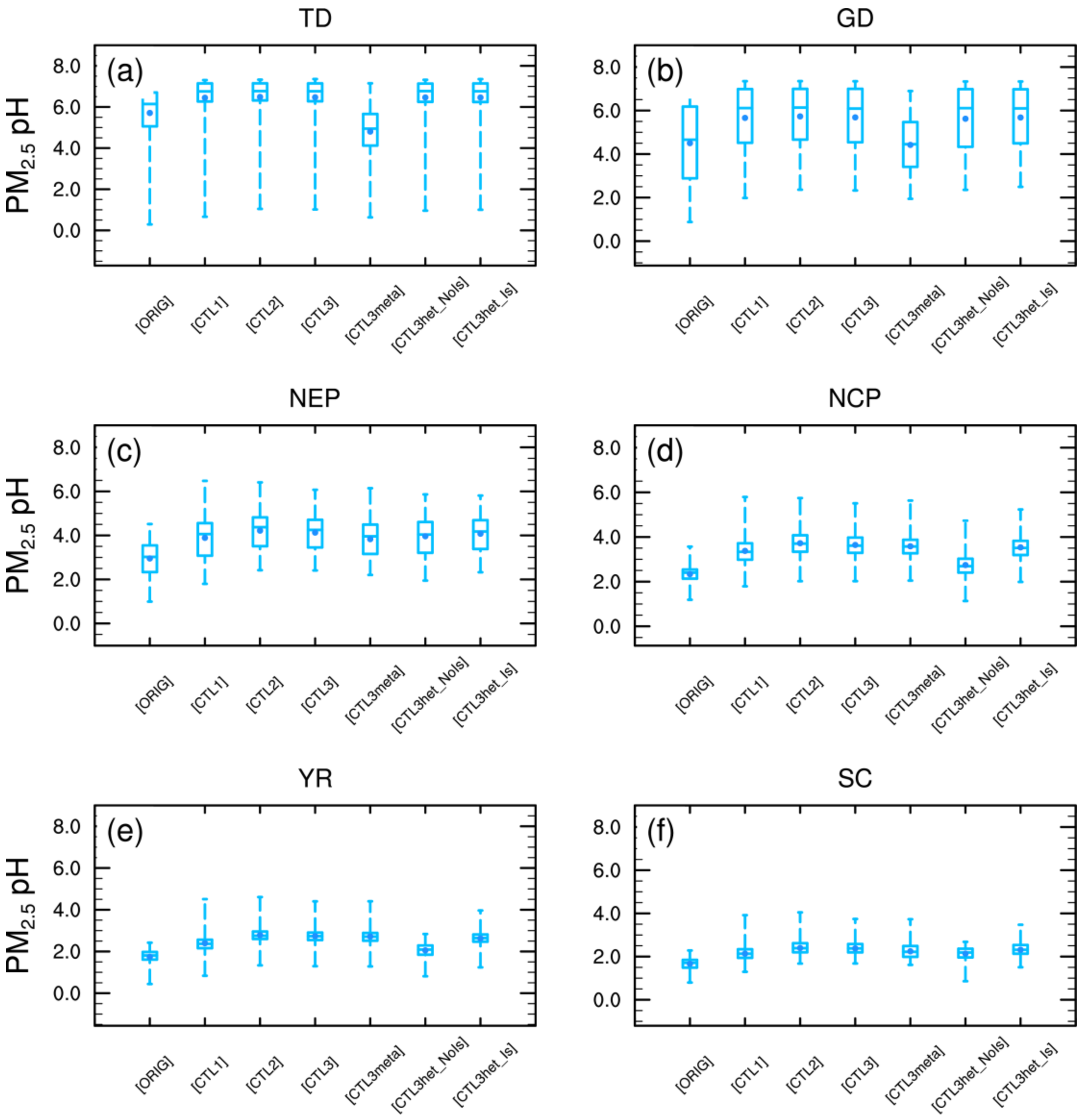

Figure S5. Boxplots of surface $PM_{2.5}$ pH simulated by each scenarios over (a) TD, (b) GD, (c) NEP, (d) NCP, (e) YR, (f) SC. The boxes represent, from top to bottom, the 75th, 50th, and 25th percentiles of statistical data. The whiskers represent, from top to bottom, the minimum and the maximum, and the solid circles represent the mean values.

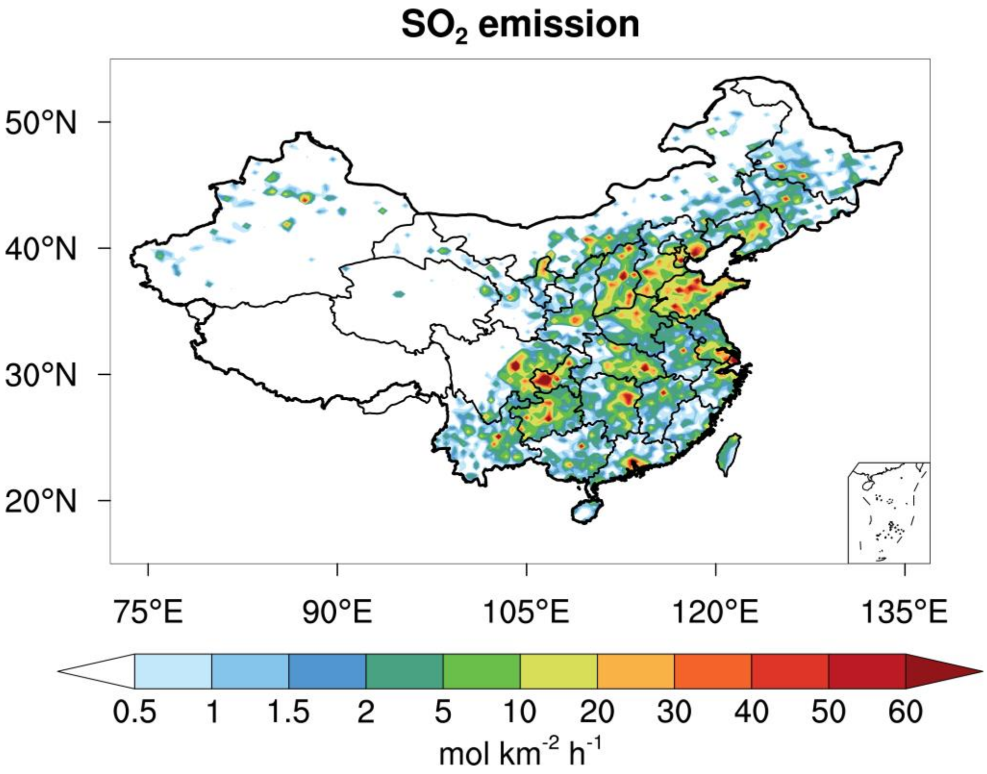

Figure S6. Spatial distribution of SO_2 emission from the MEIC China inventory during the study period of 15 October 2014 - 02 November 2014.

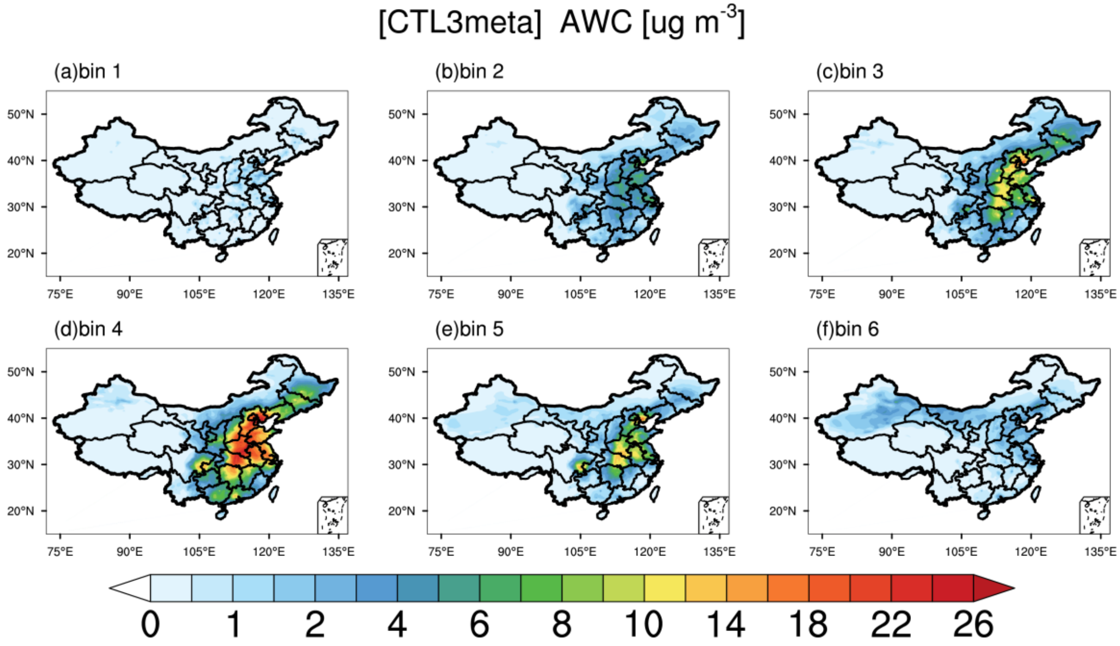

Figure S7. Spatial distributions of AWC (μg m^{-3}) during the study period of 15 October 2014 - 02 November 2014 predicted by CTL3meta scenario for six size bins. (a) Bin 1 for 0.039-0.078 μm diameter, (b) Bin 2 for 0.078-0.156 μm diameter, (c) Bin 3 for 0.156-0.312 μm diameter, (d) Bin 4 for 0.312-0.625 μm diameter, (e) Bin 5 for 0.625-1.25 μm diameter, (f) Bin 6 for 1.25-2.5 μm diameter.

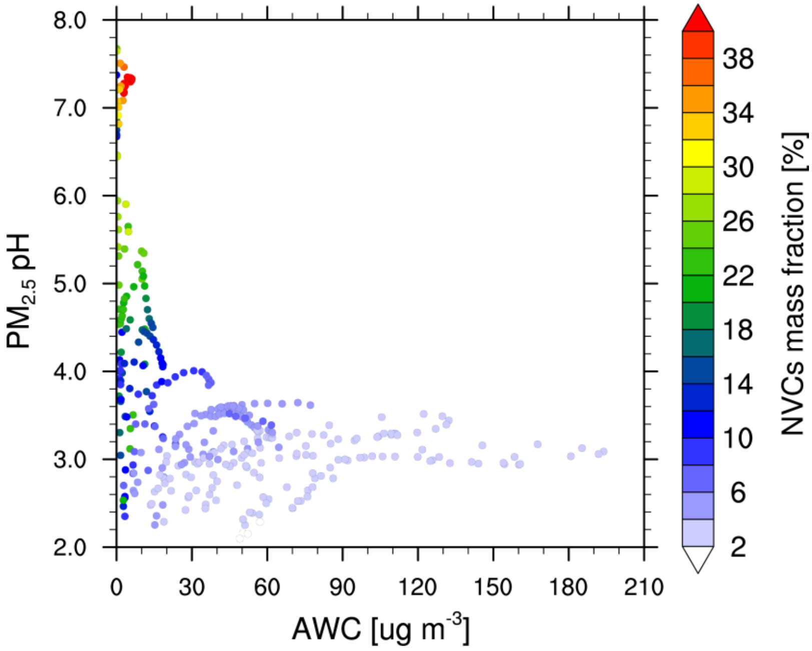

Figure S8. Scatter plots of modeled surface $PM_{2.5}$ pH vs. AWC (μg m^{-3}) colored with NVCs mass fraction (%) from CTL3meta scenario for data at Beijing site during the study period of 15 October 2014 - 02 November 2014.

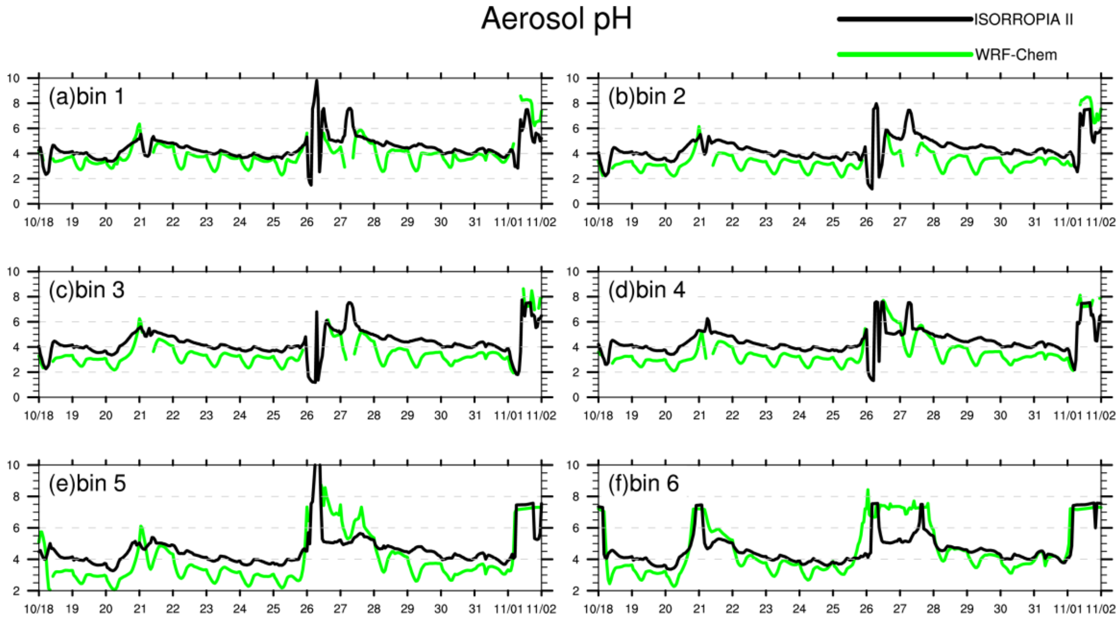

Figure S9. Time series of aerosol pH (bin01-bin06) calculated by WRF-Chem (CTL3meta, green line) and ISORROPIA II (black line) at the surface in Beijing. ISORROPIA II (“forward” mode, assuming metastable) was run with WRF-Chem simulated hourly chemical concentrations along with T and RH.

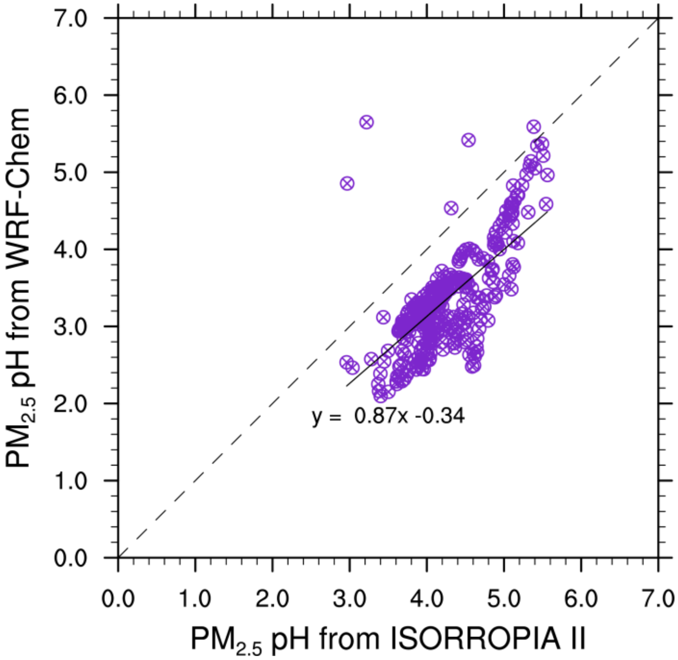

Figure S10. PM$_{2.5}$ pH predicted by WRF-Chem against the corresponding pH predicted using ISORROPIA II for the data presented in Fig. S9. PM$_{2.5}$ pH is calculated using LWC-weighted average from bin 01~bin 06. The dashed line denotes the 1:1 line. Linear regression fit is shown.

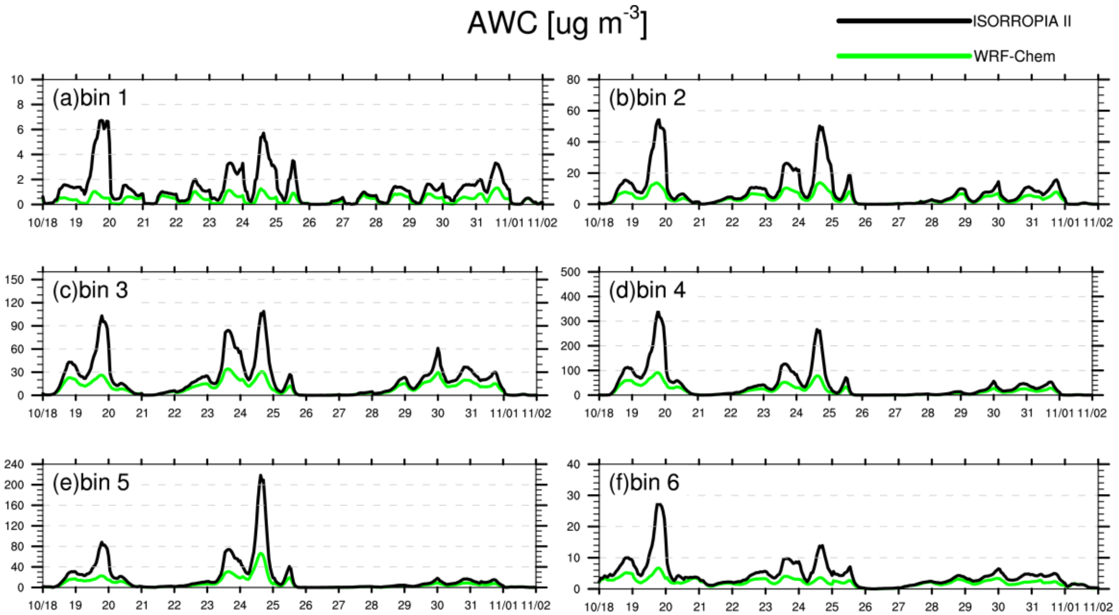

Figure S11. Same as Fig. S9, but for AWC (μg m^{-3}).

References

Clifton, C. L., Altstein, N., and Huie, R. E.: Rate constant for the reaction of nitrogen dioxide with sulfur(IV) over the pH range 5.3-13, Environ. Sci. Technol., 22, 586-589, https://doi.org/10.1021/es00170a018, 1988.

Hoffmann, M. R., and Calvert, J. G.: Chemical Transformation Modules for Eulerian Acid Deposition Models. Volume 2. The Aqueous-Phase Chemistry., Atmospheric Sciences Research Laboratory, Office of Research and Development, US Environmental Protection Agency, 1985.

Ibusuki, T., and Takeuchi, K.: Sulfur-Dioxide Oxidation by Oxygen Catalyzed by Mixtures of Manganese(II) and Iron(III) in Aqueous-Solutions at Environmental Reaction Conditions, Atmos. Environ., 21, 1555-1560, https://doi.org/10.1016/0004-6981(87)90317-9, 1987.

Lee, Y. N., and Schwartz, S. E.: Kinetics of oxidation of aqueous sulfur(IV) by nitrogen dioxide, Conference: 4. international conference on precipitation scavenging, dry deposition and resuspension, Santa Monica, CA, USA, 29 Nov 1982, ; Brookhaven National Lab., Upton, NY (USA), Medium: X; Size: Pages: 15 pp., 1982.

Liu, T., Clegg, S. L., and Abbatt, J. P. D.: Fast oxidation of sulfur dioxide by hydrogen peroxide in deliquesced aerosol particles, Proc. Natl. Acad. Sci. U. S. A., 117, 1354-1359, https://doi.org/10.1073/pnas.1916401117, 2020.

Mcardle, J. V., and Hoffmann, M. R.: Kinetics and Mechanism of the Oxidation of Aquated Sulfur-Dioxide by Hydrogen-Peroxide at Low pH, J. Phys. Chem., 87, 5425-5429, https://doi.org/10.1021/j150644a024, 1983.

Pye, H. O. T., Nenes, A., Alexander, B., Ault, A. P., Barth, M. C., Clegg, S. L., Collett, J. L., Fahey, K. M., Hennigan, C. J., Herrmann, H., Kanakidou, M., Kelly, J. T., Ku, I. T., McNeill, V. F., Riemer, N., Schaefer, T., Shi, G. L., Tilgner, A., Walker, J. T., Wang, T., Weber, R., Xing, J., Zaveri, R. A., and Zuend, A.: The acidity of atmospheric particles and clouds, Atmos. Chem. Phys., 20, 4809-4888, https://doi.org/10.5194/acp-20-4809-2020, 2020.

Zaveri, R. A., Easter, R. C., Fast, J. D., and Peters, L. K.: Model for Simulating Aerosol Interactions and Chemistry (MOSAIC), J. Geophys. Res.-Atmos., 113, https://doi.org/10.1029/2007JD008782, 2008.